BUREAU OF RECLAMATION

Technical Memorandum No. 86-68330-2024-10

Event Relative Location and Updated Earthquake Catalog Paradox Valley Seismic network

Paradox Valley Unit, Colorado

Colorado River Basin Salinity Control Program
Upper Colorado Basin Region

U.S. Department of the Interior **August 2024**

Mission Statements

The U.S. Department of the Interior protects and manages the Nation's natural resources and cultural heritage; provides scientific and other information about those resources; honors its trust responsibilities or special commitments to American Indians, Alaska Natives, and affiliated Island Communities.

The mission of the Bureau of Reclamation is to manage, develop, and protect water and related resources in an environmentally and economically sound manner in the interest of the American public.

Technical Memorandum No. 86-68330-2024-10

Event Relative Location and Updated Earthquake Catalog Paradox Valley Seismic Network

Paradox Valley Unit, Colorado

Colorado River Basin Salinity Control Program
Upper Colorado Basin Region

Prepared by:

Bureau of Reclamation
Technical Service Center
Denver, Colorado

U.S. Department of the Interior **August 2024**

Technical Memorandum No. 86-68330-2024-10

Event Relative Location and Updated Earthquake Catalog Paradox Valley Seismic Network

Paradox Valley Unit, Colorado

Colorado River Basin Salinity Control Program
Upper Colorado Basin Region

LISA BLOCK

Digitally signed by LISA BLOCK
Date: 2024.08.28 12:47:50 -06'00'

Prepared by: Lisa Block
Geophysicist, Geomorphology and Seismology Group, 86-68330

Peer Review

GLENDA BESANA-OSTMAN

Digitally signed by GLENDA BESANA-OSTMAN
Date: 2024.08.28 13:06:25 -06'00'

Peer reviewed by Glenda Besana-Ostman
Geologist, Geomorphology and Seismology Group, 86-68330

Acronyms and Abbreviations

1-D	one-dimensional
3-D	three-dimensional
aeqd	azimuthal equidistant (projection)
BOR	Bureau of Reclamation
GPS	Global Positioning System
GRS80	Geodetic Reference System 1980 (ellipsoid)
km	kilometers
M_D	duration magnitude
mi	miles
M_W	moment magnitude
PVSN	Paradox Valley Seismic Network
PVU	Paradox Valley Unit
rms	root-mean-square
RSN	Ridgway Seismic Network
SLU	Saint Louis University
U.S.	United States
V_P	P-wave velocity
V_S	S-wave velocity
V_P/V_S	Vp-to-Vs ratio

Symbols

>	greater than
≥	greater than or equal to
<	less than
≤	less than or equal to
Δt	time difference

Contents

Page

1.0 Introduction....1

2.0 Event Relative Location....3
2.1 Time Difference Data....3
2.1.1 Waveform Cross-correlations....3
2.1.2 Absolute Arrival Times....5
2.1.3 Station GPS Timing....6
2.2 Method....7
2.3 Results....10

3.0 PVSN Combined Catalog....16

4.0 References....19

Tables

Table Page

Table 1: Stations, Dates, and Orientations of Mis-aligned Seismometers at PVSN.... 4

Table 2: Dates When Stations Had Unreliable Timing.... 6

Table 3: Earthquakes Fixed During the Relative Location Inversions.... 9

Table 4: PVU-induced Earthquakes For Which Magnitudes From Other Sources.... 17

Figures

Figure Page

Figure 1: Locations of the PVSN seismic stations, PVU injection well, and epicenters of earthquakes ≤ 10 km deep recorded through 2023.... 2

Figure 2: Absolute locations from the PVSN local earthquake catalog, earthquakes that were fixed during the event relative location inversions, and relative location inversion regions.... 8

Figure 3: Combined PVSN earthquake catalog. Relative locations (a-quality events) are plotted with filled circles color-coded by hypocenter elevation, and absolute locations (b-quality events) are plotted as gray dots.... 11

Figure 4: Hypocenters in inversion region 1: (a) initial absolute hypocenters color-coded by hypocenter elevation and (b) final combined catalog with relative hypocenters color-coded by hypocenter elevation and absolute hypocenters plotted as gray dots 12

Figure 5: Hypocenters in inversion region 2: (a) initial absolute hypocenters color-coded by hypocenter elevation and (b) final combined catalog with relative hypocenters color-coded by hypocenter elevation and absolute hypocenters plotted as gray dots 13

Figure 6: Hypocenters in inversion region 3: (a) initial absolute hypocenters color-coded by hypocenter elevation and (b) final combined catalog with relative hypocenters color-coded by hypocenter elevation and absolute hypocenters plotted as gray dots 14

Figure 7: Hypocenters in inversion region 4: (a) initial absolute hypocenters color-coded by hypocenter elevation and (b) final combined catalog with relative hypocenters color-coded by hypocenter elevation and absolute hypocenters plotted as gray dots 15

Figure 8: Geographical extent of the PVSN local earthquake catalog electronic attachment. 18

1.0 Introduction

The Bureau of Reclamation (Reclamation) operates the Paradox Valley Seismic Network (PVSN) in western Colorado (Figure 1). PVSN monitors earthquakes induced by a single deep injection well at Reclamation's Paradox Valley Unit (PVU), a component of the Colorado River Basin Salinity Control Program (Block et al., 2024). Installation of PVSN began in 1983, and the data have been continuously recorded and archived since 1985. When PVU injection began in July 1991, PVSN consisted of 14 stations. Thirteen of these stations had single-component, vertically oriented short-period seismometers, while the station closest to the injection well (PV11) had three components. Reclamation has upgraded PVSN several times over the years, and the network currently consists of 20 digital three-component broadband seismic stations and three strong motion sites. In six years of pre-injection monitoring (1985 to mid-1991), PVSN recorded only one naturally occurring local earthquake (within ~25 km of the injection well). Since injection began in July 1991, PVSN has recorded more than 11,000 induced earthquakes (Block et al., 2024).

In the 1980s and early 1990s, readily available regional one-dimensional (1-D) velocity models were used for calculating hypocenters of local earthquakes recorded by PVSN. As more PVU-induced earthquakes were recorded, the arrival time data were used to compute local 1-D, and later three-dimensional (3-D), velocity models to use in the hypocenter calculations. Station corrections were also computed as part of model development. As earthquakes occurred in new areas and additional seismic stations were added to PVSN, these models were periodically updated. The most recent model update was performed in early-to-mid 2024 and is documented in Block (2024b). Improvements in the most recent model compared to previous implementations include incorporation of well log velocities from 23 boreholes in the Paradox Valley area and computation of an independent 3-D S-wave velocity (V_S) model. In previous implementations, the velocity structure was parameterized by a 3-D P-wave velocity (V_P) model and a 1-D V_P/V_S model. Independent 3-D P-wave and S-wave velocity models were produced for the most recent model because many more S-wave arrival times are available now than in the past, due to upgrades of all seismic stations to three-component sensors (Block et al., 2024).

Absolute hypocenters of the local earthquakes in the PVSN database were recomputed with the updated velocity model and corresponding station corrections, using manually determined arrival times. Relative hypocenters were then computed using the new velocity model and travel time differences between pairs of events derived from waveform cross-correlations. This report provides a description of the waveform cross-correlation and event relative hypocenter procedures (also referred to less formally as event relative location), as well as a description of the attached earthquake catalog. A combined earthquake catalog that contains either a relative or absolute hypocenter for each event is provided as an electronic attachment. The catalog contains local earthquakes recorded by PVSN from 1985 to 2023.

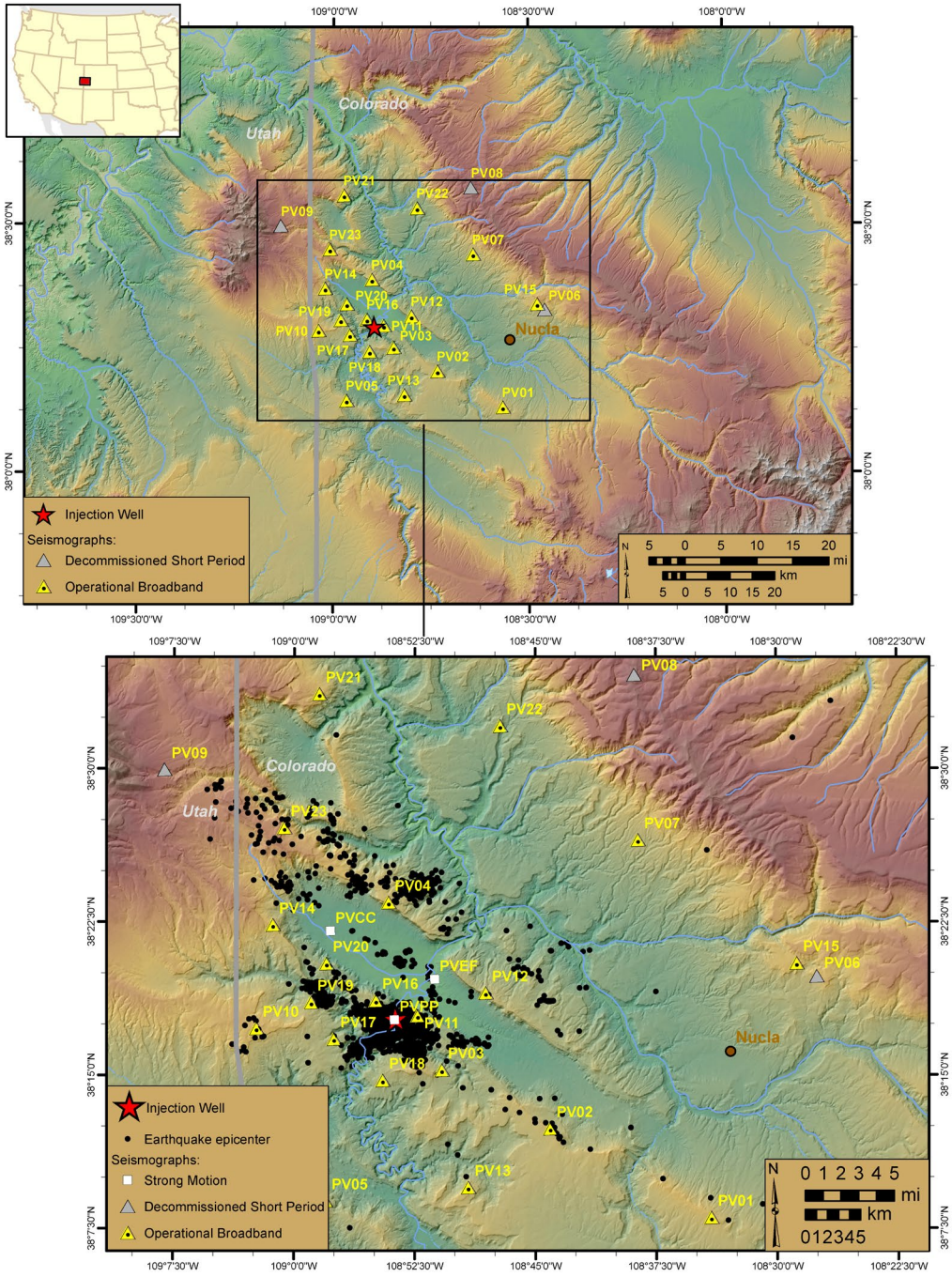

Figure 1: Locations of the PVSN seismic stations, PVU injection well, and epicenters of earthquakes ≤ 10 km deep recorded through 2023. Station PV06 was decommissioned in 1994 due to repeated vandalism and replaced by PV15. Stations PV08 and PV09, which were at locations with poor site response, were decommissioned in 2015 after the network was upgraded from short-period sensors to broadband instrumentation. The vertical gray line is the Colorado-Utah boundary. Figure from Block et al. (2024).

2.0 Event Relative Location

2.1 Time Difference Data

2.1.1 Waveform Cross-correlations

Precise time differences between seismic waveforms recorded at the same station for pairs of earthquakes are computed using time-domain cross-correlation. P-wave time differences (Δts) are computed only from vertical-component data, while S-wave time differences are computed only from horizontal-component data. For the horizontal components, cross-correlations are performed between waveforms having the same orientation only (East or North), and no component rotation based on ray path geometry is performed. Time differences from both East- and North-component data at the same station may be included in the event relative location inversions for the same event pair. Cross-correlations are initially performed for event pairs with separation distances up to 8 km, but most of the data from the largest event separation distances are later discarded based on cross-correlation data quality factors or separation criteria applied during the event relative location inversions, as described later.

Prior to cross-correlation, the waveforms are filtered using a third-order Bessel bandpass filter with corner frequencies of 0.8 and 25 Hz for vertical-component data and 0.6 and 15 Hz for horizontal-component data. The filter is applied in the forward and reverse directions for zero-phase filtering. In addition, corrections are applied to the data for operational changes in the seismic network. This includes rotating the horizontal components into a North-East orientation for time periods when the seismometer was known to be mis-aligned. The stations, time periods, and seismometer orientations used for these corrections are listed in Table 1. Note that for one of the stations, the seismometer was mis-aligned by almost 180°. The other correction applied to the waveforms is to reverse the East and North component names for the analog short-period data at station PV16 recorded from October 1 2000 to the time the short-period seismometers were removed from this site in July 2015. These data stream names were apparently reversed during a network upgrade in 2000.

Only cross-correlations between waveforms recorded with the same type of seismometer (analog short-period, digital broadband, or strong motion) are used. For a discussion of the types of instrumentation installed at PVSN and their time periods of operation, see Block et al. (2024) or the latest PVSN annual report available at https://www.usbr.gov/uc/progact/paradox/. In earlier implementations of the relative location inversion, time differences derived from cross-correlations between waveforms recorded by the original PVSN analog short-period seismometers and the later digital broadband seismometers had been included. However, small timing discrepancies were observed between different instrumentation types simultaneously deployed at the same site, even after appropriate filtering of the waveforms into a common frequency band. Timing corrections had been determined and applied during the relative location inversions. At many of the sites, the short-period and broadband instrumentation operated

Table 1: Stations, Dates, and Orientations of Mis-aligned Seismometers at PVSN

Station and Seismometer Type	Time Period	Orientation of North Seismometer Component
PV04 digital broadband	original installation (May 2007) to 8/23/2007 18:00 UTC	N28°W
PV08 analog short-period	re-installation (Oct. 2007) to 10/25/2008 18:00	N9°E
PV12 digital broadband	original installation (Nov. 2005) to 10/24/2007 23:00	S5°E
PV12 digital broadband	10/24/2007 23:00 to 10/24/2008 22:00	N4°E
PV17 digital broadband	original installation (Nov. 2005) to 10/24/2007 18:00	N5°E

side-by-side for a number of years, and this data provided good constraints on the timing differences. Sufficient data are now available from each instrumentation type to make inclusion of cross-correlations between waveforms from different instrumentation types unnecessary. Therefore, cross-correlations between waveforms recorded by different instrumentation types are no longer included.

For each waveform pair, cross-correlations are performed using three window lengths: 1.5 s, 1.0 s, and 0.5 s for P waves and 2.0 s, 1.5 s, and 1.0 s for S waves. The manually determined arrival time is used to position each window, with 25% of the window before the arrival time and 75% of the window after the arrival time. If an S-wave arrival time is available for an event and the end of the P-wave cross-correlation window is greater than the corresponding S-wave arrival time, then that window length is not used for the P-wave cross-correlation. If even the smallest window length is too long to end before the S-wave arrival time, then the P-wave cross-correlation window length is adjusted to end at the S-wave arrival time. A minimum absolute cross-correlation coefficient of 0.7 is required to retain the time difference from a given window length.

In order to increase the accuracy of the time differences computed from the cross-correlations, each cross-correlation computation is performed in two steps. First, the cross-correlation is performed with the original waveform data over a relatively large range of lags (from -25% of the window length to +25% of the window length). Then the waveforms are resampled (by linear interpolation) at 50 times their original sample interval of 0.01 s, resulting in a new sampling interval of 0.0002 s, and the cross-correlation is repeated for a small range of lags (from -5 original sample intervals to +5 original sample intervals), around the lag value corresponding to the maximum absolute cross-correlation value from the first pass. This data resampling allows the accuracy of the computed arrival time differences to be less than the original sample interval of the recorded data. The derived time difference corresponds to the lag of the maximum absolute cross-correlation value from this second pass.

In addition to the value of peak (or trough) of the cross-correlation function, two other parameters are computed and output as a measure of the quality of the cross-correlation function: the width of the cross-correlation peak (or trough) and the absolute value of the ratio the largest sidelobe to the main peak. The width of the cross-correlation peak is measured as the time lag difference between the two points on either side of the cross-correlation peak where the cross-correlation function has half its peak value. To compute the sidelobe-to-main peak ratio, the four nearest peaks and troughs are examined (two on either side of the main peak), and the peak or trough with the largest absolute value is used to compute the ratio.

The time differences initially derived from the cross-correlations are subsequently post-processed to eliminate multiple time differences for a given waveform pair and to identify and eliminate time differences from poor quality cross-correlations. If a time difference is available from only one window length for a given waveform pair, then a minimum absolute cross-correlation coefficient of 0.8 is required. Time differences from single cross-correlations with absolute peak values less than this criterion are eliminated. If cross-correlations are available from multiple window lengths for a given waveform pair, then the absolute difference in Δts from the two cross-correlations having the highest absolute cross-correlation values is required to be less than 0.01 s. In addition, all cross-correlation functions are checked to ensure that the main peak is not extremely broad and that the sidelobes are not excessively large compared to the main peak. Time differences from cross-correlations whose peaks have widths > 0.5 s are rejected. Also, if the maximum absolute cross-correlation value is ≥ 0.75 and the absolute ratio of the largest sidelobe to the main peak of the cross-correlation function is ≥ 0.95, the time difference is eliminated. If the maximum absolute cross-correlation value is < 0.75, then time differences with ratios > 0.90 are eliminated.

Once this post-processing is complete, the quality of the data set used in the relative location inversions is further improved by only including P-wave time differences from cross-correlations with peak absolute values ≥ 0.75 and S-wave time differences from cross-correlations with peak absolute values ≥ 0.7. The threshold is higher for P-waves than for S-waves because the P-wave cross-correlations appear to be more susceptible to error, such as from cycle-skipping, than the S-wave cross-correlations. (Many of the waveforms recorded by PVSN are from low-magnitude earthquakes that may have emergent P-waves or low signal-to-noise ratio.)

2.1.2 Absolute Arrival Times

No absolute arrival times are directly included in the relative location inversions. However, time differences computed from manually determined absolute P-wave arrival times (with high pick weights) are included in the inversions for earthquakes with duration magnitude ≥ 3.0, to supplement the time differences from waveform cross-correlation. Many waveforms from these larger earthquakes are clipped and therefore do not produce good cross-correlations, especially for data recorded prior to about 2010 when short-period analog seismometers were still in use at most PVSN seismic stations. For the two earthquakes with moment magnitude ≥ 4.0, only time differences from absolute arrival times are used, because the different frequency content of the

largest-magnitude earthquakes appears to degrade their cross-correlations with smaller-magnitude events. Time differences derived from absolute arrival times are down-weighted by a factor of 100 in the inversions, relative to time differences from waveform cross-correlations.

2.1.3 Station GPS Timing

There are some known time periods during the history of PVSN when station timing was not reliable. For the analog short-period seismometers originally used in the network, all stations received timing from a single Global Positioning System (GPS) antenna. There is one known time period in late 2010 when this antenna malfunctioned and the stations did have reliable timing. For the digital broadband stations installed later, each station has its own GPS antenna. For several years after these stations were installed, individual GPS antennas occasionally malfunctioned and lost timing. (This issue was eventually resolved by adding a watchdog feature to the station electronics that monitors the signal output from the GPS antenna and reboots the antenna if the output ceases.) The stations and time periods for which GPS timing is known to be unreliable are listed in Table 2.

Table 2: Dates When Stations Had Unreliable Timing

Station	Component Type[1]	Date Range
All	analog short-period (‘E’)	11/18/2010 - 12/8/2010
PV04	digital broadband (‘H’)	2/24/17 - 4/24/17
PV05	digital broadband (‘H’)	8/1/2013 - 8/2/2013
PV07	digital broadband (‘H’)	4/26/2015 - 7/31/2015
PV07	digital broadband (‘H’)	5/30/2016 - 6/28/2016
PV12	digital broadband (‘H’)	prior to 5/9/2007
PV12	digital broadband (‘H’)	10/22/18 - 10/24/18
PV12	digital broadband (‘H’)	4/21/2019 - 5/2/2019
PV14	digital broadband (‘H’)	4/15/2019 - 5/1/2019
PV16	digital broadband (‘H’)	9/7/2010 - 10/15/2010
PV16	digital broadband (‘H’)	6/4/2018 - 8/27/2018
PV17	digital broadband (‘H’)	prior to 5/9/2007
PV17	digital broadband (‘H’)	2/15/2009 - 4/26/2009
PV18	digital broadband (‘H’)	3/1/2012 - 5/10/2012
PV18	digital broadband (‘H’)	6/15/2012 - 10/22/2012
PV18	digital broadband (‘H’)	12/25/2016 - 1/16/2017
PV22	digital broadband (‘H’)	2/21/2014 - 3/20/2014
PV22	digital broadband (‘H’)	3/3/2015 - 3/26/2015
PV22	digital broadband (‘H’)	6/18/2015 - 8/5/2015
PV22	digital broadband (‘H’)	2/20/18 - 4/10/18
PV23	digital broadband (‘H’)	11/25/2016 - 12/09/2016

[1] The letter in parentheses is the data stream identifier in the waveform files

Time differences are eliminated from the event relative locations if either of the waveforms in a given pair has unreliable timing, based on the information in Table 2. Time differences derived from both waveform cross-correlations and manually determined arrival times are eliminated.

2.2 Method

The event relative hypocenter inversion is performed in the local Cartesian coordinate system used for development of PVSN's local 3-D velocity model. This coordinate system has its origin at the PVU injection well, and the horizontal axes are rotated 55° counterclockwise so that they align with the trend of Paradox Valley (Block, 2024b). The transformation between geographic (latitude and longitude) and Cartesian coordinates is done using the software package *proj* (PROJcontributors, 2019), with an azimuthal equidistant (aeqd) projection and the Geodetic Reference System 1980 (GRS80) ellipsoid.

The nonlinear relative hypocenter inversion is performed by iteratively solving the linearized problem. The recently developed 3-D local velocity model is used for determining travel times and ray paths (Block, 2024b). The initial absolute earthquake locations are also determined using this model. The problem is formulated as a least squares inversion, but residual weighting can be used to approximate an L1-norm optimization. A mathematical description of the inversion method is provided in Block et al. (2020).

The PVSN local earthquake catalog from 1985 to 2023 contains over 11,000 earthquakes. These events occur over an area elongated in the northwest-southeast direction that is approximately 50 km long and 23 km wide (Figure 2). The highest density of earthquakes occurs within about 3 km of the PVU injection well. The more distant earthquakes occur in many dispersed clusters. Because of the large number of earthquakes and their occurrence over a large area where event-station ray coverage varies, the relative locations are performed separately in different regions (Figure 2, white rectangles). This limits the inversion matrices to more manageable sizes (which may still contain tens of millions of non-zero elements) and also allows for different event inclusion criteria to be used in areas with different event density and ray coverage.

Absolute earthquake locations are not well constrained by time difference data alone, and therefore additional constraints on the absolute earthquake locations are required. A center-of-mass constraint can be used, but this constraint is most applicable to relatively small regions with a single or small number of earthquake clusters. When used over large areas with multiple earthquake clusters, the center-of-mass constraint does not prevent earthquake clusters from shifting relative to their positions determined from absolute arrival times. Absolute arrival times can be directly included in the relative event location inversion, but this increases the computational resources required. It can also be difficult to properly adjust the weighting

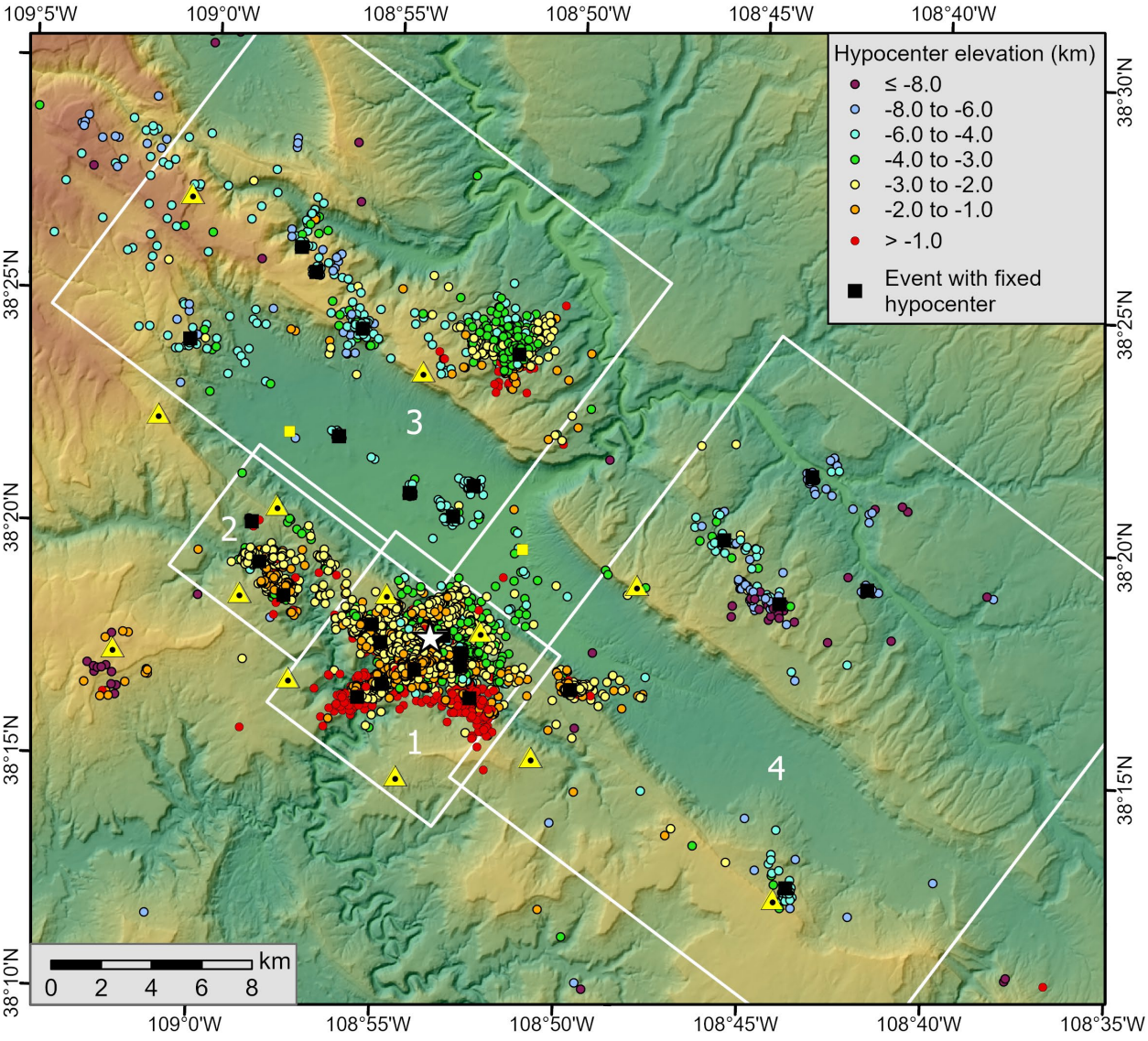

Figure 2: Absolute locations from the PVSN local earthquake catalog (filled circles, color-coded by hypocenter elevation), earthquakes that were fixed during the event relative location inversions (filled black squares), and relative location inversion regions (numbered white rectangles). The white star is the PVU injection well, the yellow triangles are PVSN broadband seismic stations, and the yellow squares are PVSN strong motion sites.

between the absolute arrival time data and the time difference data; if the absolute data are weighted too strongly, the relative locations are degraded. In the PVSN relative hypocenter inversions, the absolute positions of earthquake clusters are constrained by fixing the initial absolute hypocenters of a few widely spaced earthquakes. All earthquakes must tie, either directly or indirectly (possibly through multiple event pairs), to an event with a fixed location to be retained in the inversions. The earthquakes with fixed hypocenters are shown in Figure 2 (black squares) and listed in Table 3.

Table 3: Earthquakes Fixed During the Relative Location Inversions

Inversion Region	Event ID	Date	Time (UTC)	Latitude (deg.)	Longitude (deg.)	Elevation (km)	M_D[1]	Pickfile Name
1	1145	7/22/1991	0:46:08	38.296911	-108.888752	-2.812	0.2	910722004557p
1	2648	1/11/1998	8:51:48	38.293875	-108.917432	-2.098	0.7	980111085135p
1	2899	3/3/1998	16:24:03	38.300052	-108.921714	-2.289	1.0	980303162350p
1	2939	3/8/1998	3:09:47	38.286287	-108.880861	-1.844	1.6	980308030935p
1	4959	12/13/1999	23:52:52	38.290975	-108.880686	-3.524	2.1	991213235240p
1	7235	5/17/2012	0:32:32	38.273848	-108.927093	-0.209	1.2	120517003216p
1	9801	3/14/2019	20:14:36	38.284259	-108.901597	-2.161	1.8	190314201413p
1	12180	12/17/2020	20:24:30	38.278828	-108.916367	-2.202	1.7	201217202407p
1	13451	3/11/2024	2:13:49	38.274834	-108.875996	-0.641	1.5	240311021326p
2	6006	2/7/2008	19:26:26	38.321071	-108.973963	-2.384	1.3	080207192609p
2	6210	11/10/2009	18:04:35	38.30935	-108.962361	-2.012	1.9	091110180417p
2	13348	10/12/2023	19:06:39	38.335334	-108.97801	-0.944	0.1	231012190617p
3	6380	10/14/2010	19:59:23	38.399972	-109.009177	-4.919	1.6	101014195907p
3	7489	11/28/2013	20:45:37	38.339761	-108.8864	-4.577	0.6	131128204522p
3	7548	11/2/2014	16:03:35	38.366968	-108.939775	-4.288	0.8	141102160319p
3	8475	9/5/2018	22:44:10	38.347591	-108.906682	-4.216	0.0	180905224340p
3	8479	9/10/2018	9:47:02	38.351003	-108.877728	-4.936	1.4	180910094640p
3	10520	6/11/2019	9:11:01	38.405797	-108.930924	-4.481	0.9	190611091040p
3	10970	9/24/2019	6:33:16	38.398633	-108.859063	-3.728	1.6	190924063258p
3	12624	12/12/2021	1:33:37	38.434242	-108.959924	-4.925	1.1	211212013316p
3	8452	7/31/2018	22:38:25	38.425472	-108.952892	-5.208	0.5	180731223804p
4	8090	5/1/2017	22:13:58	38.279116	-108.830461	-2.075	1.4	170501220745p
4	8384	3/8/2018	16:28:58	38.318577	-108.696848	-7.541	1.6	180308162837p
4	8593	11/13/2018	7:39:26	38.334768	-108.762722	-4.419	0.9	181113073905p
4	11691	1/13/2020	10:06:00	38.312576	-108.73663	-6.741	1.2	200113100421p
4	12378	4/11/2021	8:56:20	38.358564	-108.72365	-6.526	0.5	210411085603p
4	12574	10/10/2021	2:28:35	38.210864	-108.729298	-4.807	1.1	211010022817p

[1] Duration magnitude

Several relative location inversions are progressively performed in each region (Figure 2). For the initial inversions, an L2 norm is used to avoid down-weighting data with large residuals that may represent reliable signals rather than noise. For later inversions, an L1 norm is used. Residual cut-offs are employed for both individual time difference residuals and root-mean-square (rms) time difference residuals for individual earthquakes. Data that produce residuals above these cut-offs are eliminated during each iteration of the inversions. Initial inversions use large residual cut-offs, and these cut-offs are decreased for later inversions. A maximum allowable event separation distance is specified for each inversion, as well as a separation distance above which the data are downweighted (using a linear taper). In general, larger distance criteria are used for regions with lower earthquake density, while smaller distance

criteria are used in areas with high earthquake density. In addition, larger distance criteria are often used for the initial inversions in a region and decreased for later inversions in that same region as clusters become more compact. Sometimes, relative locations of events that are eliminated during the final inversion using the smallest allowable event separation distance are retrieved from the previous inversion and still included in the final set of relative locations. This allows for fine-tuning alignments of events in small clusters (using small separation distances) while also retaining relative locations of events that tied in previously (using somewhat larger separation distances). The maximum separation distances used for the inversions performed here range from 0.25 km to 6 km.

Only earthquakes with fairly well constrained hypocenters are included in the relative hypocenter inversions. For inversion region 1 (surrounding the PVU injection well, Figure 2), where earthquake density is high and event-station ray coverage is good, earthquakes are retained in the inversions if they meet the following minimum criteria: time differences (either P-wave or S-wave) available from at least 6 stations; maximum azimuthal gap in time difference data ≤ 160°; and distance to the closest station having time difference data divided by hypocenter depth ≤ 2. For the other inversion regions, where earthquake density is lower and event-station ray coverage is not as good, the maximum azimuthal gap is increased to 200°, and the maximum distance to the closest station divided by hypocenter depth is increased to 3. All hypocenter inclusion criteria are re-evaluated after each iteration of the inversion. Because each earthquake shares time difference data with other events, whenever an earthquake is eliminated from the inversion, the criteria for all other events are re-evaluated. The ties between all events are also re-evaluated to ensure that all earthquakes still tie (directly or indirectly) to an earthquake with a fixed location.

2.3 Results

Of the more than 11,000 local earthquakes in the PVSN catalog, 9,771 earthquakes (~86%) tie into the relative locations. In the near-well area (inversion region 1, Figure 3), 90% of the events tie into the relative locations. The earthquakes with relative locations are assigned a quality factor of ‘a’. For those earthquakes that do not tie into the relative locations, the absolute locations are used and are assigned a quality factor of ‘b’. This combined PVSN earthquake catalog is plotted in Figure 3.

The relative locations exhibit more compact earthquake clusters than the absolute locations, and many of the relative locations form distinct lineations. Hypocenters in the final combined catalog are compared to the absolute hypocenters for each inversion region in Figure 4 to Figure 7. The re-activated fault systems and stress states interpreted from these earthquake lineations are discussed in other Reclamation reports and publications (Ake et al., 2005; Block et al., 2020; Block et al., 2014, 2015; Yeck et al., 2014).

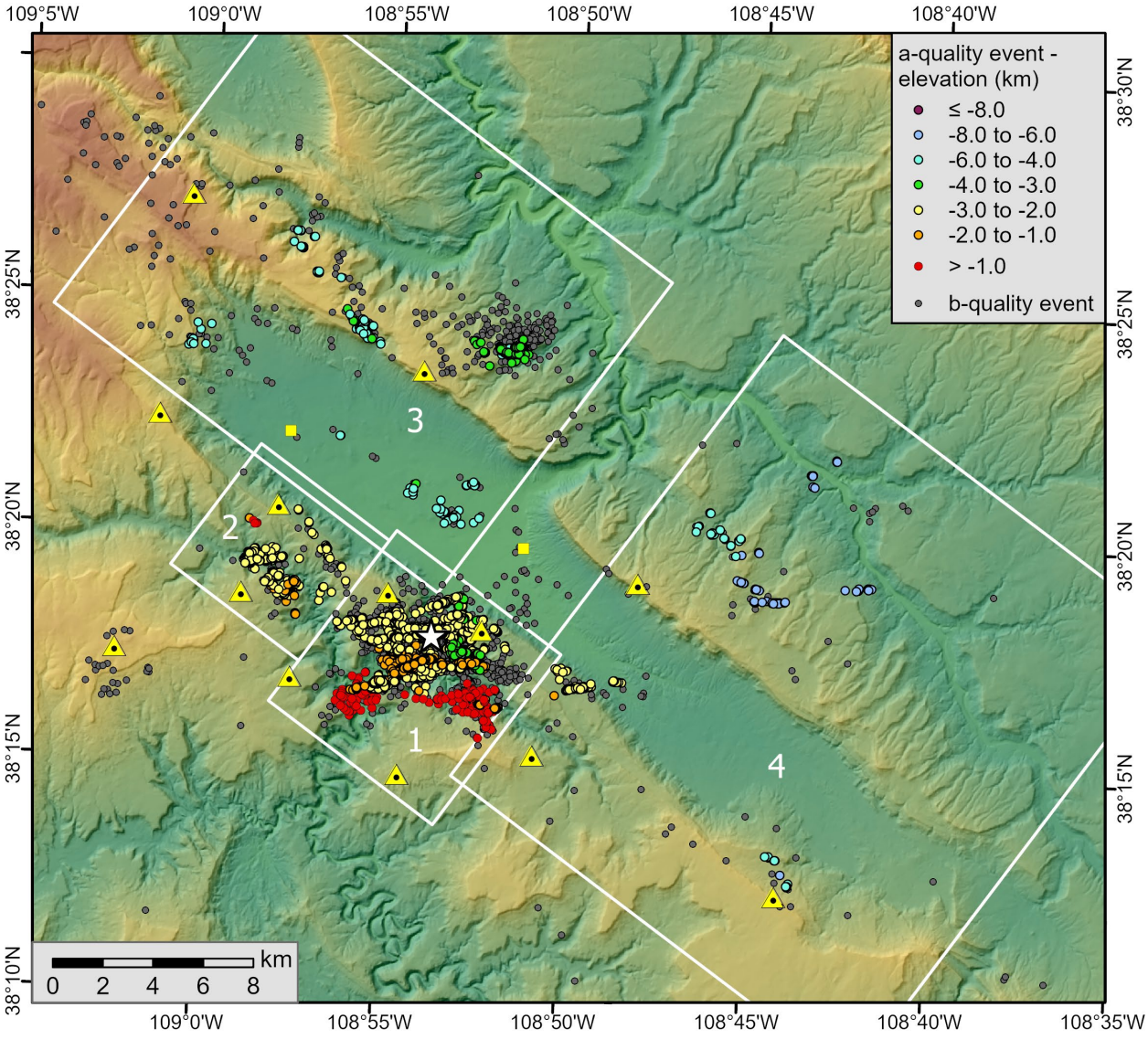

Figure 3: Combined PVSN earthquake catalog. Relative locations (a-quality events) are plotted with filled circles color-coded by hypocenter elevation, and absolute locations (b-quality events) are plotted as gray dots. The relative location inversion regions are shown as numbered white rectangles. The white star is the PVU injection well, the yellow triangles are PVSN broadband seismic stations, and the yellow squares are PVSN strong motion sites.

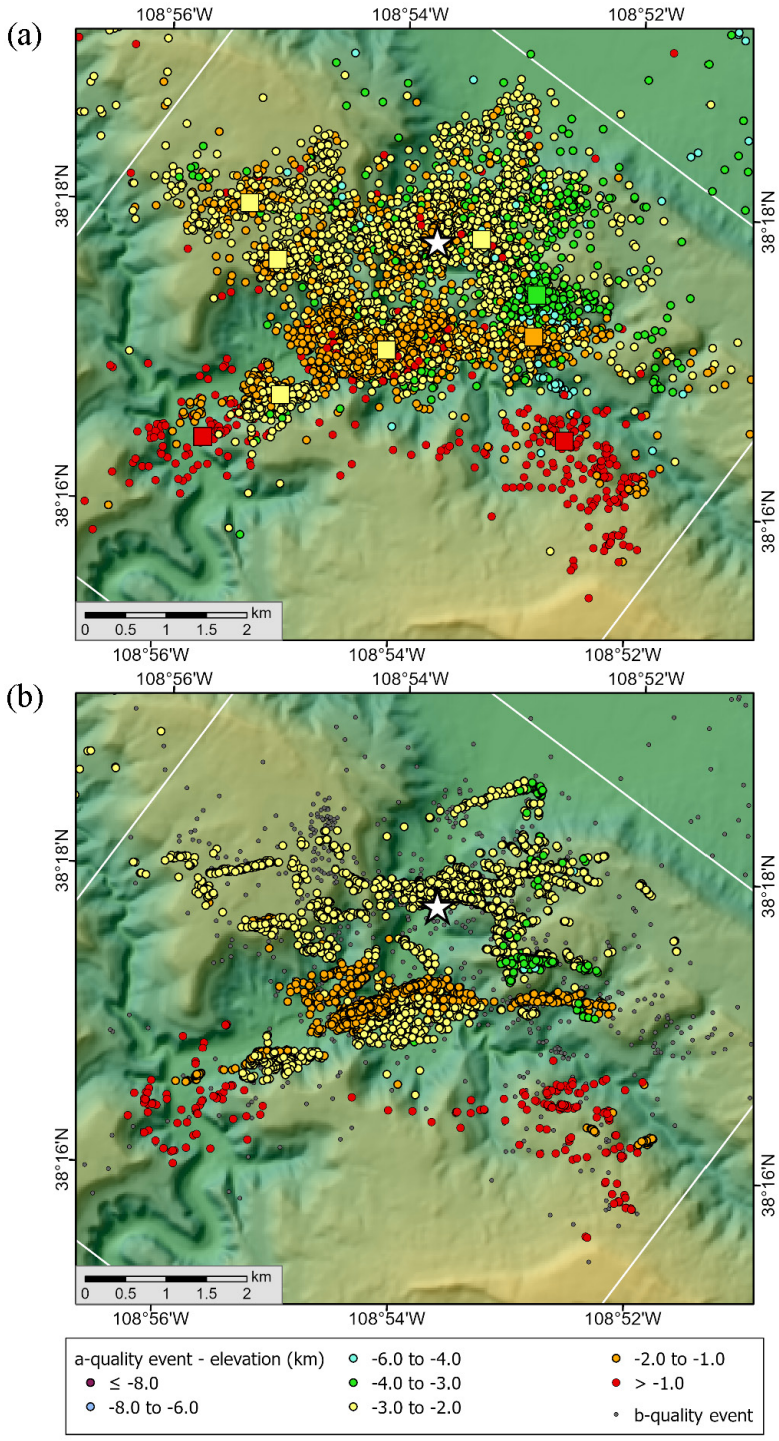

Figure 4: Hypocenters in inversion region 1 (white rectangle): (a) initial absolute hypocenters color-coded by hypocenter elevation and (b) final combined catalog with relative hypocenters color-coded by hypocenter elevation and absolute hypocenters plotted as gray dots. Hypocenters fixed during the relative locations are shown in (a) as squares color-coded by hypocenter elevation, using the same color scale as for the other hypocenters. The white star is the PVU injection well.

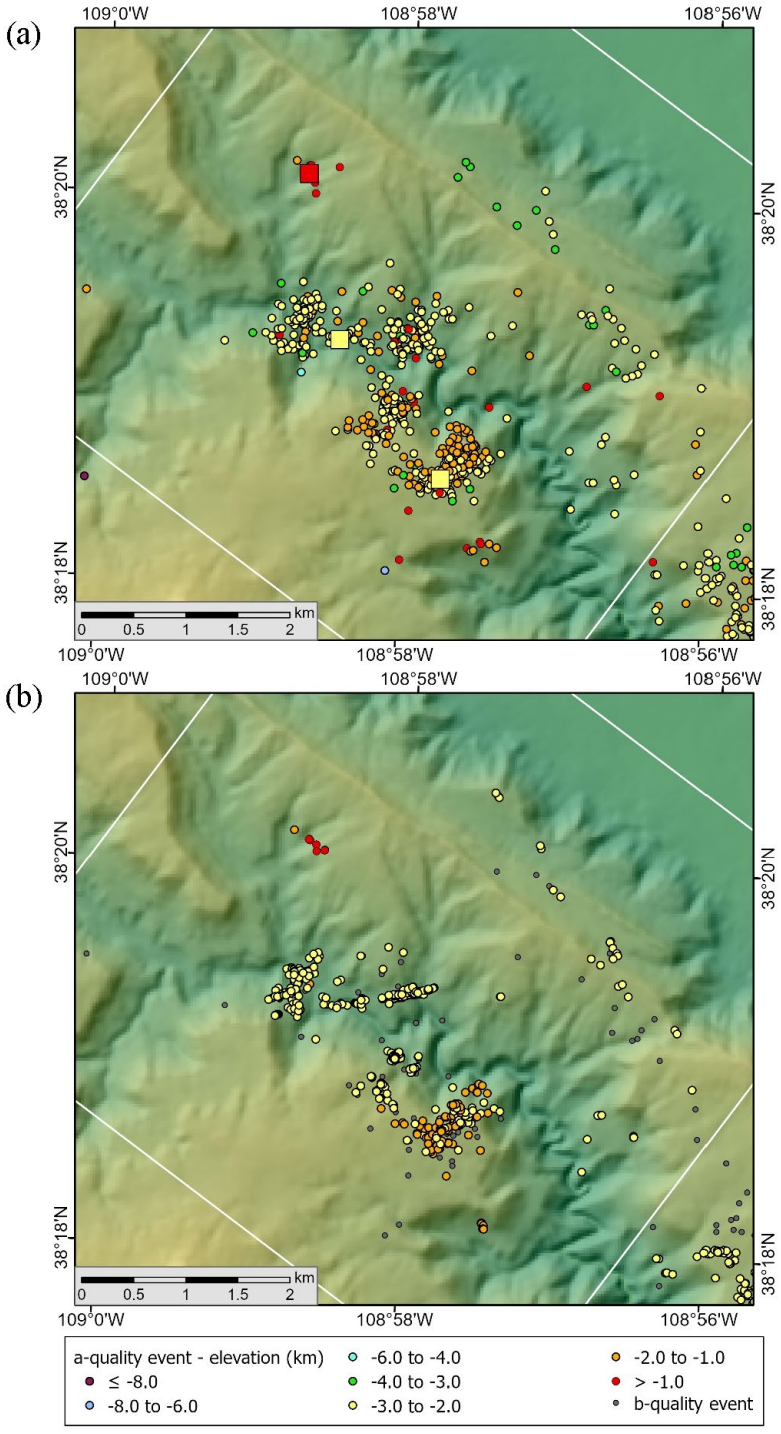

Figure 5: Hypocenters in inversion region 2 (white rectangle): (a) initial absolute hypocenters color-coded by hypocenter elevation and (b) final combined catalog with relative hypocenters color-coded by hypocenter elevation and absolute hypocenters plotted as gray dots. Hypocenters fixed during the relative locations are shown in (a) as squares color-coded by hypocenter elevation, using the same color scale as for the other hypocenters.

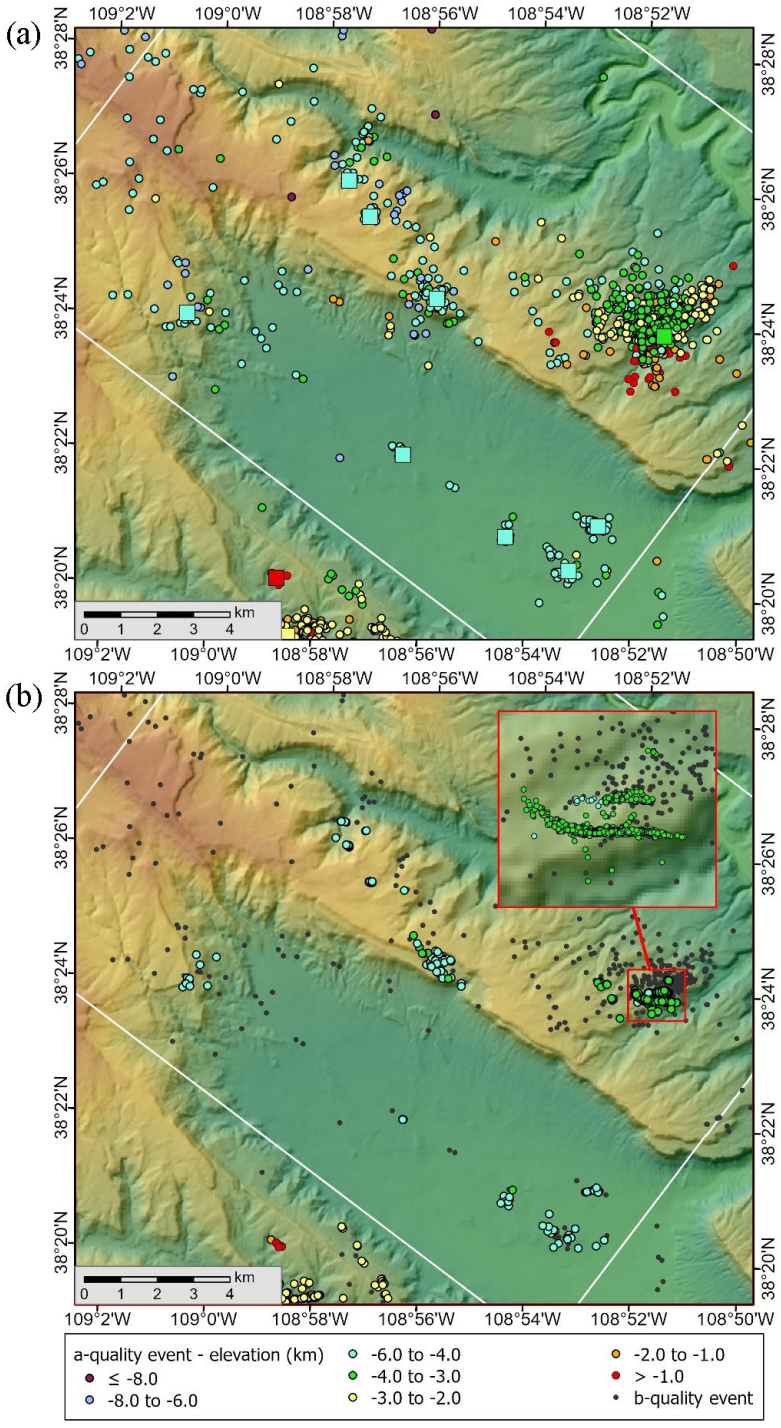

Figure 6: Hypocenters in inversion region 3 (white rectangle): (a) initial absolute hypocenters color-coded by hypocenter elevation and (b) final combined catalog with relative hypocenters color-coded by hypocenter elevation and absolute hypocenters plotted as gray dots. Hypocenters fixed during the relative locations are shown in (a) as squares color-coded by hypocenter elevation, using the same color scale as for the other hypocenters.

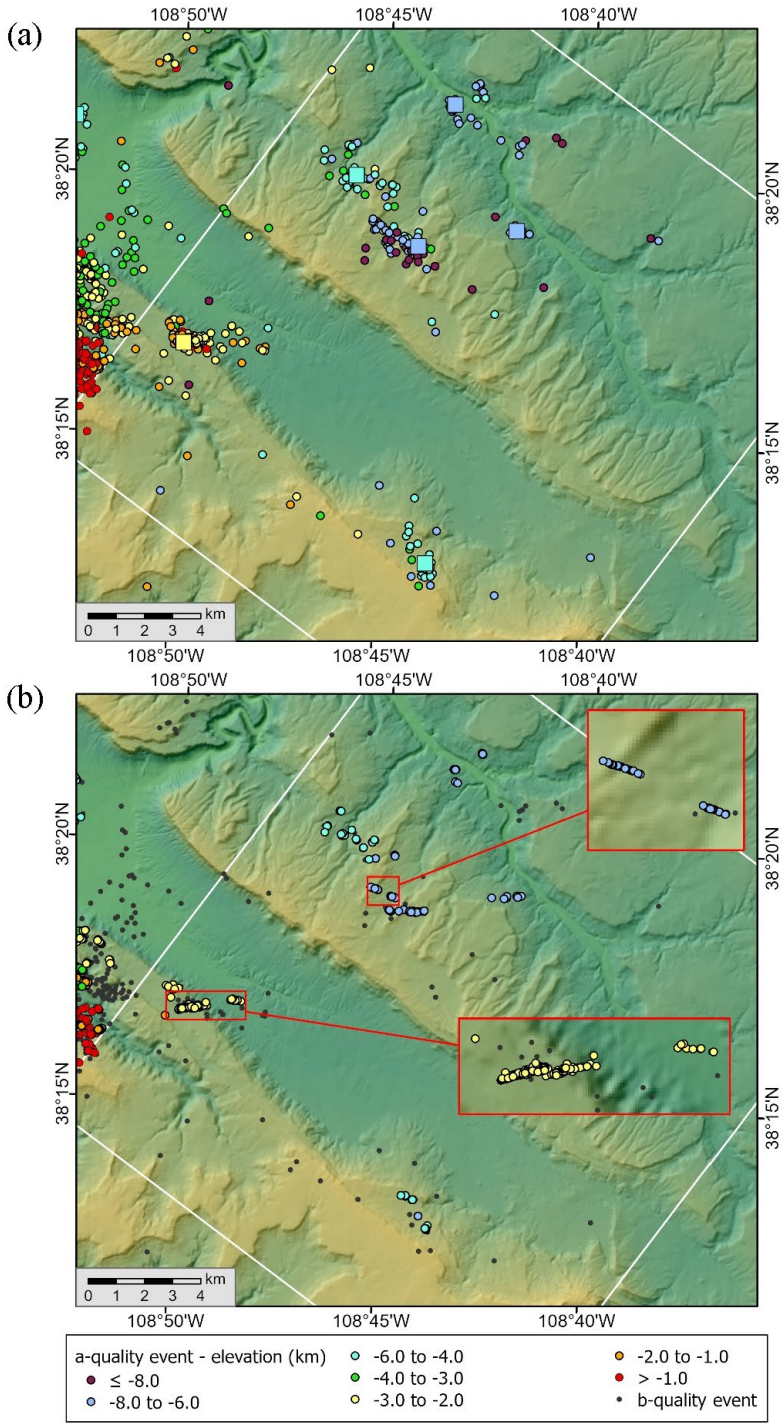

Figure 7: Hypocenters in inversion region 4 (white rectangle): (a) initial absolute hypocenters color-coded by hypocenter elevation and (b) final combined catalog with relative hypocenters color-coded by hypocenter elevation and absolute hypocenters plotted as gray dots. Hypocenters fixed during the relative locations are shown in (a) as squares color-coded by hypocenter elevation, using the same color scale as for the other hypocenters.

3.0 PVSN Combined Catalog

A PVSN combined earthquake catalog is provided as an electronic attachment to this report. This catalog contains earthquakes that occurred within approximately 10 km of the perimeter of PVSN from 1985 through 2023 (Figure 8). Identified explosions are excluded from the catalog.

The earthquakes in the attached catalog were detected and their locations computed primarily using data from PVSN. However, data from the nearby Ridgway Seismic Network (RSN), also operated by Reclamation, supplemented the PVSN data for some of the events that occurred from 1985 to 2007. The relative location inversions only use data from PVSN, and their starting absolute hypocenters presented on earlier maps in this report were computed only using PVSN data. Hence, there could be some differences between the absolute hypocenters plotted on the earlier maps in this report and the final b-quality hypocenters presented in Figure 8 and included in the electronic attachment.

This catalog contains one hypocenter for each earthquake. Relative (a-quality) hypocenters are provided for the earthquakes that tie into the relation location inversions. For the earthquakes that do not tie into the relative location inversions, the absolute (b-quality) hypocenters are provided. In the attached catalog, 9,771 hypocenters (86% of the events) have a-quality hypocenters, and the remaining 1,607 earthquakes have b-quality hypocenters.

Duration and moment magnitudes computed using only PVSN data (and possibly some RSN data for early events) are provided in the attached catalog. For some of the larger PVU-induced earthquakes, especially those recorded prior to the upgrade of PVSN stations to digital broadband instrumentation, these magnitudes may not be the best ones available. The duration magnitudes (Md) saturate above approximately Md 3.0. In addition, for time periods when most stations still had short-period instrumentation (prior to about 2010), many of the waveforms for earthquakes above Md 3.0 are clipped, and therefore robust moment magnitudes (Mw) cannot be computed using only PVSN data. With the current broadband instrumentation, a substantial number of waveforms are clipped for earthquakes with magnitudes above ~Mw 4.0 – Mw 4.5. A list of the larger PVU-induced earthquakes for which magnitudes from other sources (such as the U. S. Geologic Survey, University of Utah Seismograph Stations, or Saint Louis University) should be considered to supplement the information in the attached catalog are given in Table 4. For the earliest of these earthquakes, the waveform durations were manually manipulated to make the computed Md values equal to local or moment magnitudes available from outside sources (Table 4, footnote 1). This practice is no longer used, but, as of the date of this report, the durations for these earthquakes have not been corrected. Magnitudes for the earthquakes listed in Table 4 from multiple sources are included in previous Reclamation reports and publications (Block et al., 2020; Block, 2024a; Block et al., 2014; Wood et al., 2016; Yeck et al., 2014).

Table 4: PVU-induced Earthquakes For Which Magnitudes From Other Sources Should be Considered to Supplement the Information in the Attached Earthquake Catalog

Event ID	Date	Time	Md in Attached Catalog	Mw in Attached Catalog
4570	6/3/1999	15:35:34	3.5[1]	
4675	7/6/1999	22:05:45	3.5[1]	
5141	5/27/2000	21:58:19	3.8[1]	
5774	11/7/2004	6:55:00	4.0[1]	3.78
7381	1/24/2013	4:46:39	3.1	4.27
8652	3/4/2019	17:22:51	3.1	4.55

[1] Waveform durations were manipulated to increase the computed Md value

The earthquake catalog file contains the following columns:

Event_ID: Identification number of event

Year: Earthquake origin time year
Month: Earthquake origin time month
Day: Earthquake origin time day
Hour: Earthquake origin time hour
Minute: Earthquake origin time minute
Second: Earthquake origin time second

Latitude_(deg): Hypocenter latitude in decimal degrees North.
Longitude_(deg): Hypocenter longitude in decimal degrees; negative values are West
Elevation_(m): Hypocenter elevation in meters with respect to mean sea level

Md: Duration Magnitude; the duration magnitudes saturate above approximately Md 3.0.
Mw: Moment Magnitude; computed using only PVSN data.

Quality: Indicates whether the hypocenter was computed with a relative location method (quality = ‘a’) or an absolute location method (quality=’b’).

RMS_residual_(s): Root-mean-square (rms) time residual in seconds. For b-quality events, this is the rms of the absolute time residuals. For a-quality events, this is the rms of the time difference residuals.
Nabstimes: Number of arrival times used to compute the absolute location of b-quality events. (Zero for a-quality events.)
Neventpairs: Number of event pairs providing time differences for the relative location of a-quality events. (Zero for b-quality events.)
Ntimediffs: Number of time differences used to compute the relative location of a-quality events. (Zero for b-quality events.)

Nstations: Number of stations providing data for the hypocenter calculations, either in terms of absolute arrival times (for b-quality events) or time differences (for a-quality events).
Maxgap_(deg): Maximum azimuthal gap in ray coverage to the nearest integer degree. For the event relative location (a-quality events), this considers data for all event pairs.
Min_dist/depth: Horizontal distance to the closest seismic station providing data for the hypocenter calculation divided by the hypocenter depth.

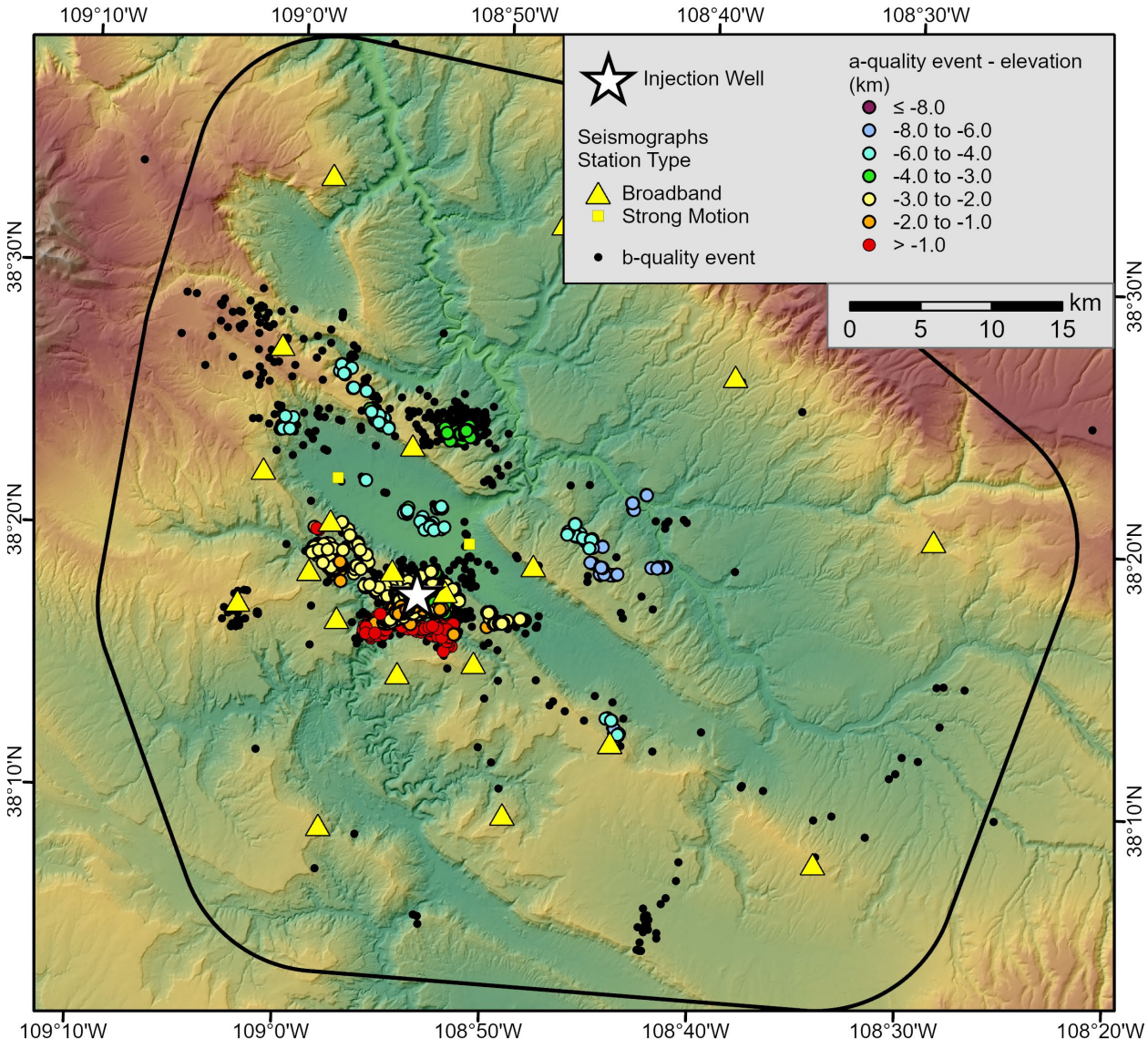

Figure 8: Geographical extent of the PVSN local earthquake catalog electronic attachment. A-quality earthquakes with relative locations (filled circles color-coded by hypocenter elevation) and b-quality earthquakes with absolute locations (black dots) from 1985 to 2023 are included in the attachment.

4.0 References

Ake, J., Mahrer, K., O'Connell, D., and Block, L., 2005, Deep-injection and closely monitored induced seismicity at Paradox Valley, Colorado: *Bulletin of the Seismological Society of America*, v. 95, no. 2, p. 664-683.

Block, L., Besana-Ostman, G., and Wood, C., 2020, *Analysis of the March 4, 2019 Earthquake and Its Aftershocks:* Technical Memorandum No. 86-68330-2020-07, Bureau of Reclamation, Denver, Colorado, 149 pp.

Block, L., Wood, C. K., Schwarzer, J., Kang, J. B., Besana-Ostman, G., and Ball, J., 2024, *2023 Annual Report, Paradox Valley Seismic Network, Paradox Valley Unit, Colorado:* Technical Memorandum No. 86-68330-2024-3, Bureau of Reclamation, Denver, Colorado, 88 pp.

Block, L. V., 2024a, *Analyses of the Fall 2020 Seismicity Swarm, Paradox Valley Unit, Colorado*: Technical Memorandum No. 86-68330-2024-8, Bureau of Reclamation, Denver, Colorado, 99 pp.

Block, L. V., 2024b, *Development of a New Velocity Model for the Paradox Valley Area, Paradox Valley Unit, Colorado*: Technical Memorandum No. 86-68330-2024-7, Bureau of Reclamation, Denver, Colorado, 122 pp.

Block, L. V., Wood, C. K., Yeck, W. L., and King, V. M., 2014, The 24 January 2013 ML 4.4 Earthquake near Paradox, Colorado, and Its Relation to Deep Well Injection: *Seismological Research Letters*, v. 85, no. 3, p. 609-624.

Block, L. V., Wood, C. K., Yeck, W. L., and King, V. M., 2015, Induced seismicity constraints on subsurface geological structure, Paradox Valley, Colorado: *Geophysical Jounal International*, v. 200, p. 1172-1195.

PROJcontributors, 2019, PROJ coordinate transformation software library: *Open Source Geospatial Foundation: URL* https://proj.org.

Wood, C. K., Block, L. V., King, V. M., and Yeck, W. L., 2016, *The ML 4.4 Earthquake of January 24, 2013, Near Paradox, Colorado, and Implications for Near-term Injection Operations:* Technical Memorandum 86-68330-2013-12, Bureau of Reclamation, pp. 151.

Yeck, W. L., Block, L. V., Wood, C. K., and King, V. M., 2014, Maximum magnitude estimations of induced earthquakes at Paradox Valley, Colorado, from cumulative injection volume and geometry of seismicity clusters: *Geophysical Journal International*, v. 200, no. 1, p. 322-336.